A novel strategy to identify the critical conditions for growth-induced instabilities

A. Javili[a,*], P. Steinmann[a], E. Kuhl[b]

[a] *Chair of Applied Mechanics, University of Erlangen–Nuremberg, Egerlandstr. 5, 91058 Erlangen, Germany*
[b] *Stanford University, 496 Lomita Mall, Stanford, CA 94305, USA*

Abstract

Geometric instabilities in living structures can be critical for healthy biological function, and abnormal buckling, folding, or wrinkling patterns are often important indicators of disease. Mathematical models typically attribute these instabilities to differential growth, and characterize them using the concept of fictitious configurations. This kinematic approach towards growth-induced instabilities is based on the multiplicative decomposition of the total deformation gradient into a reversible elastic part and an irreversible growth part. While this generic concept is generally accepted and well established today, the critical conditions for the formation of growth-induced instabilities remain elusive and poorly understood. Here we propose a novel strategy for the stability analysis of growing structures motivated by the idea of replacing growth by prestress. Conceptually speaking, we kinematically map the stress-free grown configuration onto a prestressed initial configuration. This allows us to adopt a classical infinitesimal stability analysis to identify critical material parameter ranges beyond which growth-induced instabilities may occur. We illustrate the proposed concept by a series numerical examples using the finite element method. Understanding the critical conditions for growth-induced instabilities may have immediate applications in plastic and reconstructive surgery, asthma, obstructive sleep apnoea, and brain development.

Keywords: Growth, morphogenesis, residual stress, prestress, stability analysis, instabilities

1. Introduction

Structural instabilities in the form of creases, folds, or wrinkles are inherent to living matter. In many living systems, the formation of structural instabilities is critical to biological function, e.g., to increase the surface-to-volume ratio of the system. Typical examples are wrinkles in skin (Buganza et al., 2011), villi in the intestine (Balbi and Ciarletta, 2013), or folds in the developing brain (Bayly et al., 2013). In other biological systems, however, the formation of structural instabilities can be a critical hallmark of disease, e.g., when associated with a narrowing lumen. The most prominent example of this latter category is the folding of the mucous membrane in asthmatic airways (Wiggs et al., 1997). It is thus not surprising that the mathematical modeling of folding in tubular organs (Ciarletta and Ben Amar, 2012), in particular the modeling of the folding mucous membrane (Moulton and Goriely, 2011; Li et al., 2011; Xie et al., 2013), has drawn increasing scientific attention within the past decade.

Continuum approaches towards the formation of geometric instabilities in living systems typically adopt the concept of finite growth (Rodriguez et al., 1994). This kinematic approach towards growth is based on the introduction of a fictitious growth configuration (Garikipati, 2009) and on the multiplicative decomposition of the deformation gradient into a reversible elastic and an irreversible growth part (Taber, 1995). Mathematically speaking, in this approach, growth is represented through a second order, isotropic (Himpel et al., 2005), transversely isotropic (Zöllner et al., 2012a), orthotropic (Göktepe et al., 2010), or generally anisotropic. As discussed in a recent review article on growth (Ambrosi, 2011), the evolution of this growth tensor is typically either morphogenetically driven (Li et al., 2012) or mechanically driven (Menzel and Kuhl, 2012).

*Corresponding author. Tel.: +49 (0)9131 85 28502, Fax: +49 (0)9131 85 28503
Email address: ali.javili@ltm.uni-erlangen.de (A. Javili)

Here we focus on morphogentically driven growth and on its role in the formation of structural instabilities. The first rigorous mathematical analyses of growth-induced morphogenetic instabilities studied the failure models of a shrinking spherical shell (Goriely and BenAmar, 2005) and of a growing spherical shell under external pressure (Ben Amar and Goriely, 2005). Motivated by the clinical problem of mucosal folding during chronic airway wall remodeling, recent studies explored the buckling of single-layered (Moulton and Goriely, 2011) and double-layered (Cao et al., 2012; Jin et al., 2011) hollow cylindrical tubes. In realistic airway wall geometries, the thickness of the folding inner layer is typically orders of magnitude smaller than the cylindrical airway structure itself. Accordingly, a recent study suggested to model mucosal folding using the concept of surface growth (Papastavrou et al., 2013), an approach for which the mucosal surface itself is equipped with its own potential energy (Steinmann, 2008). A similar approach was recently proposed for the longitudinal growth in double-layered cylinders (Vandiver and Goriely, 2009) to simulate the effects of surface growth in plants (Holland et al., 2013).

Inhomogeneous growth induces a state of prestrain or residual stress (Fung, 1991). Residual stress, sometimes also referred to as prestress, is the stress in a body in the reference configuration (Menzel, 2005; Rausch et al., 2013). In the following we distinguish between two geometrically identical reference configurations, one *stress-free* and one *stressed*. We assume that the elastic deformation from the stress-free grown configuration to the stressed reference configuration results in residual stress (Rausch et al., 2013a). The theory of elasticity for a body under residual stress was first established by Biot (1939). More recently, Johnson and Hoger (1993) studied the dependence of the elasticity tensor on residual stress where the residual stress was produced by an elastic deformation (Hoger, 1986; Marlow, 1992; Hoger, 1993). The problem of dead loading in the mathematical theory of linear elasticity with initial stress (Man and Carlson, 1994) bears certain similarities to our analysis here. Ogden (1992) details on stability and uniqueness of solution of incremental boundary value problem. In Ogden (2003), he employed his generic method to soft tissues and tube extension/inflation problems with residual stresses arising from a uniform circumferential stress. For further mathematical details of symmetry, bifurcation, and instabilities in the context of elasticity with a prestressed reference configuration we refer to Bharatha and Levinson (1978); Capriz and Guidugli (1979); Wan and Marsden (1983).

In the theory of elasticity, a condition for the existence of solutions is that incremental deformations require positive energy. This physically motivated condition translates into the mathematically motivated condition of pointwise stability. In the classical theory of elasticity the pointwise stability condition corresponds to the positive definiteness of the constitutive tensor. However, in the context of prestress, we cannot simply adopt this classical pointwise stability condition for two reasons: i) The condition that the elasticity tensor is positive definite may no longer be feasible; and ii) The pointwise stability condition does not directly render the positive definiteness of the constitutive tensor, since there are several elasticity tensors, all of which are functions of the residual stress that describe residually stressed materials (Hoger, 1995). In this manuscript, we re-establish the governing equations for prestressed continua and *properly* impose the pointwise stability condition.

The necessary and sufficient conditions for the loss of well-posedness of the boundary value problem for linear elastic, homogeneous continua are the loss of ellipticity of the governing equations and the boundary complementing condition (see e.g. Simpson and Spector, 1985; Benallal et al., 1993). A sufficient condition for stability of elastic continua is the pointwise stability criterion (Hill, 1957). A general theory of uniqueness and stability for elasto-plastic solids was given by Hill (1958). The propagation of surface waves in bodies has been investigated in (Dowaikh and Ogden, 1990). Bifurcation in the form of surface instabilities has been investigated for arbitrary nonlinear elastic materials under conditions of an equibiaxial prestress (Reddy, 1982), and for plane strain (Reddy, 1983). A comprehensive study on uniqueness, loss of ellipticity, and localization for the time-discrete, rate-dependent boundary value problems with softening can be found in (Benallal et al., 2010).

In view of these considerations, the goal of this contribution is to explore the critical conditions for growth-induced instabilities in living structures. In Section 2, we illustrate the kinematics of finite growth based on the multiplicative decomposition of the total deformation gradient into an elastic and a growth part. In Section 3, we introduce the key idea of this work, the conceptual replacement of this growth part by prestress. In Section 4, we discuss the condition for strong ellipticity, the condition for pointwise stability, and the boundary complementing condition in the context of prestress. In Section 5, we illustrate these three conditions for a simple homogeneous model problem, and for the inhomogeneous problems of growth and shrinkage of a hollow cylinder and of a solid sphere. We conclude with a critical discussion and an outlook in Section 6.

1.1. Notation and definitions

The three-dimensional Euclidean space is denoted E^3. Direct notation is adopted throughout. Occasional use is made of index notation, the summation convention for repeated indices being implied. The scalar product of two vectors $\boldsymbol{a}$ and $\boldsymbol{b}$, i.e., the single contraction, is denoted $\boldsymbol{a} \cdot \boldsymbol{b} = [\boldsymbol{a}]_i[\boldsymbol{b}]_i$. The scalar product of two second-order tensors $\boldsymbol{A}$ and $\boldsymbol{B}$, i.e., the double contraction, is denoted $\boldsymbol{A} : \boldsymbol{B} = [\boldsymbol{A}]_{ij}[\boldsymbol{B}]_{ij}$. The action of a second-order tensor $\boldsymbol{A}$ on a vector $\boldsymbol{a}$ is understood as $[\boldsymbol{A} \cdot \boldsymbol{a}]_i = [\boldsymbol{A}]_{ij}[\boldsymbol{a}]_j$ and $[\boldsymbol{a} \cdot \boldsymbol{A}]_i = [\boldsymbol{a}]_j[\boldsymbol{A}]_{ji}$. The double contraction of a third-order tensor $\boldsymbol{C}$ and a second-order tensor $\boldsymbol{B}$ renders a vector according to $[\boldsymbol{C} : \boldsymbol{B}]_i = [\boldsymbol{C}]_{ijk}[\boldsymbol{B}]_{jk}$. The action of a third-order tensor $\boldsymbol{C}$ on a vector $\boldsymbol{a}$, denoted $\boldsymbol{C} \cdot \boldsymbol{a}$, is a second-order tensor with components $[\boldsymbol{C} \cdot \boldsymbol{a}]_{ij} = [\boldsymbol{C}]_{ijm}[\boldsymbol{a}]_m$. The composition of two second-order tensors $\boldsymbol{A}$ and $\boldsymbol{B}$, denoted $\boldsymbol{A} \cdot \boldsymbol{B}$, is a second-order tensor with components $[\boldsymbol{A} \cdot \boldsymbol{B}]_{ij} = [\boldsymbol{A}]_{im}[\boldsymbol{B}]_{mj}$. The tensor product of two vectors $\boldsymbol{a}$ and $\boldsymbol{b}$ is a second-order tensor $\boldsymbol{D} = \boldsymbol{a} \otimes \boldsymbol{b}$ with $[\boldsymbol{D}]_{ij} = [\boldsymbol{a}]_i[\boldsymbol{b}]_j$. The tensor product of two second-order tensors $\boldsymbol{A}$ and $\boldsymbol{B}$ is a fourth-order tensor $\boldsymbol{D} = \boldsymbol{A} \otimes \boldsymbol{B}$ with $[\boldsymbol{D}]_{ijkl} = [\boldsymbol{A}]_{ij}[\boldsymbol{B}]_{kl}$. The two standard double contractions of a fourth-order tensor $\boldsymbol{D}$ and a second-order tensor $\boldsymbol{A}$ render the second-order tensors with components $[\boldsymbol{D} : \boldsymbol{A}]_{ij} = [\boldsymbol{D}]_{ijkl}[\boldsymbol{A}]_{kl}$ and $[\boldsymbol{A} : \boldsymbol{D}]_{ij} = [\boldsymbol{A}]_{kl}[\boldsymbol{D}]_{klij}$. The non-standard double contraction of a fourth-order tensor $\boldsymbol{D}$ and a second-order tensor $\boldsymbol{A}$ renders a second-order tensor with components $[\boldsymbol{D} \,\bar{:}\, \boldsymbol{A}]_{ik} = [\boldsymbol{D}]_{ijkl}[\boldsymbol{A}]_{jl}$. The actions of a fourth-order tensor $\boldsymbol{D}$ and a vector $\boldsymbol{a}$, denoted $\boldsymbol{D} \cdot \boldsymbol{a}$, is the third-order tensor with components $[\boldsymbol{D} \cdot \boldsymbol{a}]_{ijk} = [\boldsymbol{D}]_{ijkl}[\boldsymbol{a}]_l$. The two non-standard tensor products of two second-order tensors $\boldsymbol{A}$ and $\boldsymbol{B}$ are the fourth-order tensors $[\boldsymbol{A} \,\overline{\otimes}\, \boldsymbol{B}]_{ijkl} = [\boldsymbol{A}]_{ik}[\boldsymbol{B}]_{jl}$ and $[\boldsymbol{A} \,\underline{\otimes}\, \boldsymbol{B}]_{ijkl} = [\boldsymbol{A}]_{il}[\boldsymbol{B}]_{jk}$.

2. Kinematic equations for growing continua

We consider a continuum body in the material configuration $\mathcal{B}_o \subset \mathsf{E}^3$ at time $t = 0$ and in the spatial configuration $\mathcal{B}_t$ at time $t > 0$, where $t \subset \mathcal{T} = [0, t_{\text{end}}] \subset \mathbb{R}_+$ denotes the time domain of interest. As depicted in Figure 1, we denote the surface outward unit normals in the material and spatial configurations by $\boldsymbol{N}$ and $\boldsymbol{n}$. We denote a motion of the reference placement by the orientation-preserving map $\boldsymbol{\varphi} : \mathcal{B}_o \times \mathcal{T} \to \mathsf{E}^3$ for any time $t \in \mathcal{T}$. In particular, we denote the current placement of the bulk associated with the motion $\boldsymbol{\varphi}$ by $\mathcal{B}_t = \boldsymbol{\varphi}(\mathcal{B}_o(\boldsymbol{X}), t)$ and designate its particles as $\boldsymbol{x} = \boldsymbol{\varphi}(\boldsymbol{X}, t) \in \mathcal{B}_t$. The deformation gradient $\boldsymbol{F} : T\mathcal{B}_o \to T\mathcal{B}_t$,

$$\boldsymbol{F}(\boldsymbol{X}, t) := \nabla\boldsymbol{\varphi}(\boldsymbol{X}, t) \qquad \text{with} \qquad \nabla\{\bullet\} := \{\bullet\} \otimes \frac{\partial}{\partial \boldsymbol{X}}\,, \tag{1}$$

is the invertible linear tangent map of a material line element $\mathrm{d}\boldsymbol{X} \in T\mathcal{B}_o$ to a spatial line element $\mathrm{d}\boldsymbol{x} \in T\mathcal{B}_t$, where $T\mathcal{B}_o$ and $T\mathcal{B}_t$ are the corresponding tangent spaces, and $J := \det \boldsymbol{F}$ denotes the corresponding Jacobian. The classical approach to model volumetric growth (Rodriguez et al., 1994; **?**; Göktepe et al., 2010a) is to multiplicatively decompose the deformation gradient $\boldsymbol{F}$ into an elastic part $\boldsymbol{F}_e$ and a growth part $\boldsymbol{F}_g$, see Figure 3 (left), according to

$$\boldsymbol{F} = \boldsymbol{F}_e \cdot \boldsymbol{F}_g \qquad \Rightarrow \qquad \boldsymbol{F}_e = \boldsymbol{F} \cdot \boldsymbol{F}_g{}^{-1}\,. \tag{2}$$

The goal of this manuscript is to explore whether an infinitesimal, incremental perturbation of a stable state triggers a kinematic instability. Although this analysis requires the deformation gradient $\boldsymbol{F}$ to be close to identity, the underlying framework does allow for finite growth. To adopt an infinitesimal strain theory for growth, we modify the classical multiplicative decomposition as shown in Figure 3 (right). In particular, we decompose the elastic part of the deformation gradient $\boldsymbol{F}_e$, which maps the stress-free grown configuration to the final configuration $\mathcal{B}_t$, into a deformation part $\boldsymbol{F}$ and an inverse growth part $\boldsymbol{F}_g{}^{-1}$,

$$\boldsymbol{F} = \boldsymbol{F} \cdot \boldsymbol{I} = \underbrace{\boldsymbol{F} \cdot \boldsymbol{F}_g{}^{-1}}_{\boldsymbol{F}_e} \cdot \boldsymbol{F}_g\,. \tag{3}$$

In this approach, the configuration $\mathcal{B}_s$ is only *geometrically* and not necessarily *energetically* identical to $\mathcal{B}_o$. This implies that mapping the stress-free grown configuration $\mathcal{B}_g$ onto $\mathcal{B}_s$ does, in general, induce stresses in the body. Conceptually speaking, we can understand the configuration $\mathcal{B}_s$ as the prestressed reference configuration, to which the deformation $\boldsymbol{\varphi}$ and the associated deformation gradient $\boldsymbol{F}$ are applied. For the simplest case of isotropic volume

growth, we can express the growth tensor as

$$\boldsymbol{F}_g = g\,\boldsymbol{I} \qquad \text{with} \qquad J_g = \det\,\boldsymbol{F}_g = g^3\,, \tag{4}$$

where g is a single scalar-valued growth multiplier. Growth induces a prestress in the body, and the amount of prestress depends on the magnitude of growth g. In the simplest case, the prestress $\boldsymbol{\gamma}$ is isotropic and proportional to the magnitude of growth g,

$$\boldsymbol{\gamma} = -\kappa\Big[\det\,\boldsymbol{F}_g - 1\Big]\,\boldsymbol{I} = \underbrace{-\kappa\Big[g^3 - 1\Big]}_{\gamma}\,\boldsymbol{I}\,, \tag{5}$$

where κ denotes the bulk modulus and γ is the scalar-valued isotropic prestress. The negative sign arrises from the fact that the prestress $\boldsymbol{\gamma}$ is the necessary stress to transform the grown configuration $\mathcal{B}_g$ into $\mathcal{B}_s$. Throughout this manuscript, we will use the term *growth* for the multiplier g with the understanding that g can represent both shrinkage and growth. In view of Eq. (5), we distinguish the following three scenarios,

$$\begin{cases} g < 1 \;\;\Rightarrow\;\; \gamma > 0 & \text{shrinkage,} \\ g = 1 \;\;\Rightarrow\;\; \gamma = 0 & \text{homeostatic equilibrium,} \\ g > 1 \;\;\Rightarrow\;\; \gamma < 0 & \text{growth.} \end{cases} \tag{6}$$

3. Governing equations for prestressed continua

This section focuses on characterizing the mapping from the prestressed configuration $\mathcal{B}_s$ to the current configuration $\mathcal{B}_t$ as illustrated in Figure 3 and on identifying the corresponding equilibrium and constitutive equations. Here we restrict ourselves to infinitesimal deformations, for which the deformation gradient $\boldsymbol{F}$ is close to the identity. We reparameterize $\boldsymbol{F}$ in terms of the displacement vector $\boldsymbol{u}$ via the classical relation $\boldsymbol{F} = \boldsymbol{I} + \nabla\boldsymbol{u}$. In the spirit of Section 2, we re-interpret the configurations $\mathcal{B}_s$ and $\mathcal{B}_t$ as the material and spatial configurations. In the absence of body forces, the balance of linear momentum reads

$$\mathrm{Div}\boldsymbol{P} = \boldsymbol{0} \qquad \text{in } \mathcal{B}_s\,, \tag{7}$$

where $\boldsymbol{P}$ is the Piola stress and $\mathrm{Div}\{\bullet\} := \nabla\{\bullet\} : \boldsymbol{I}$ denotes the material divergence operator. We supplement the equilibrium equation (7) by the boundary condition

$$\boldsymbol{P}\cdot\boldsymbol{N} = \boldsymbol{T}^{\mathrm{p}} \qquad \text{on } \partial\mathcal{B}_s\,, \tag{8}$$

in which $\boldsymbol{T}^{\mathrm{p}}$ denotes the externally prescribed tractions on the boundary $\partial\mathcal{B}_s$. To constitutively define the Piola stress $\boldsymbol{P}$, we introduce a the following isotropic neo-Hookean Helmholtz energy per unit volume of the prestressed reference configuration $\mathcal{B}_s$,

$$\psi = \tfrac{1}{2}\lambda\ln^2 J + \tfrac{1}{2}\mu\,[\boldsymbol{F}:\boldsymbol{F} - 3 - 2\ln J] + \gamma\,J \tag{9}$$

Here λ and μ are the standard Lamé parameters and γ is the scalar-valued prestress introduced in equation (5). The Piola stress follows from thermodynamic considerations in terms of the Helmholtz energy function (9) as thermodynamically conjugate to the total deformation gradient $\boldsymbol{F}$,

$$\boldsymbol{P} := \frac{\partial\psi}{\partial\boldsymbol{F}} = \lambda\ln J\boldsymbol{F}^{-\mathrm{t}} + \mu\,[\,\boldsymbol{F} - \boldsymbol{F}^{-\mathrm{t}}\,] + \gamma J\boldsymbol{F}^{-\mathrm{t}}\,. \tag{10}$$

To reformulate the governing equations in the context of the infinitesimal deformation theory, we linearize the Piola stress at the reference configuration $\mathcal{B}_s$ where $\boldsymbol{F} = \boldsymbol{I}$,

$$\mathrm{Lin}\,\boldsymbol{P}|_{\boldsymbol{F}=\boldsymbol{I}} = \boldsymbol{P}|_{\boldsymbol{F}=\boldsymbol{I}} + \frac{\partial\boldsymbol{P}}{\partial\boldsymbol{F}}\Big|_{\boldsymbol{F}=\boldsymbol{I}} : [\boldsymbol{F} - \boldsymbol{I}]\,. \tag{11}$$

The corresponding fourth-order tangent reads

$$\frac{\partial \boldsymbol{P}}{\partial \boldsymbol{F}} = \lambda\,[\boldsymbol{F}^{-\mathrm{t}} \otimes \boldsymbol{F}^{-\mathrm{t}} - \ln J\, \boldsymbol{F}^{-\mathrm{t}} \underline{\otimes} \boldsymbol{F}^{-1}] + \mu\,[\boldsymbol{I} \overline{\otimes} \boldsymbol{I} + \boldsymbol{F}^{-\mathrm{t}} \underline{\otimes} \boldsymbol{F}^{-1}] + \gamma J\,[\boldsymbol{F}^{-\mathrm{t}} \otimes \boldsymbol{F}^{-\mathrm{t}} - \boldsymbol{F}^{-\mathrm{t}} \underline{\otimes} \boldsymbol{F}^{-1}]\,. \tag{12}$$

and its evaluation at $\mathcal{B}_s$ results in

$$\frac{\partial \boldsymbol{P}}{\partial \boldsymbol{F}}\Big|_{\boldsymbol{F}=\boldsymbol{I}} = \lambda\,[\boldsymbol{I} \otimes \boldsymbol{I}] + \mu\,[\boldsymbol{I} \overline{\otimes} \boldsymbol{I} + \boldsymbol{I} \underline{\otimes} \boldsymbol{I}] + \gamma\,[\boldsymbol{I} \otimes \boldsymbol{I} - \boldsymbol{I} \underline{\otimes} \boldsymbol{I}] = 3[\lambda + \gamma]\,\mathbb{I}^{\mathrm{vol}} + 2[\mu - \gamma]\,\mathbb{I}^{\mathrm{sym}} + \gamma\,\mathbb{I}\,, \tag{13}$$

in terms of the fourth order tensors, $\mathbb{I}^{\mathrm{vol}} := \frac{1}{3}[\boldsymbol{I} \otimes \boldsymbol{I}]$, $\mathbb{I}^{\mathrm{sym}} := \frac{1}{2}[\boldsymbol{I} \overline{\otimes} \boldsymbol{I} + \boldsymbol{I} \underline{\otimes} \boldsymbol{I}]$, and $\mathbb{I} := \boldsymbol{I} \overline{\otimes} \boldsymbol{I}$. With the evaluation of the Piola stress $\boldsymbol{P}$ at $\boldsymbol{F} = \boldsymbol{I}$ as $\boldsymbol{P} = \gamma\,\boldsymbol{I}$ and with the minor symmetries of $\mathbb{I}^{\mathrm{vol}}$ and $\mathbb{I}^{\mathrm{sym}}$, equation (11) reads

$$\mathrm{Lin}\,\boldsymbol{P}|_{\boldsymbol{F}=\boldsymbol{I}} = \gamma\boldsymbol{I} + \Big[3[\lambda + \gamma]\mathbb{I}^{\mathrm{vol}} + 2[\mu - \gamma]\mathbb{I}^{\mathrm{sym}}\Big] : \boldsymbol{\epsilon} + \gamma\nabla\boldsymbol{u}\,, \tag{14}$$

where $\boldsymbol{\epsilon} = \nabla^{\mathrm{sym}}\boldsymbol{u}$ denotes the infinitesimal strain tensor. We can then reformulate the linearized Piola stress in terms of the effective constitutive tensor $\mathbb{C}_{\mathrm{eff}}$ in analogy to the familiar linear elasticity theory,

$$\mathrm{Lin}\,\boldsymbol{P}|_{\boldsymbol{F}=\boldsymbol{I}} = \gamma\boldsymbol{I} + \mathbb{C}_{\mathrm{eff}} : \boldsymbol{\epsilon} + \gamma\nabla\boldsymbol{u}\,, \quad \text{with} \quad \mathbb{C}_{\mathrm{eff}} := 3\lambda_{\mathrm{eff}}\,\mathbb{I}^{\mathrm{vol}} + 2\mu_{\mathrm{eff}}\,\mathbb{I}^{\mathrm{sym}}\,, \tag{15}$$

where $\lambda_{\mathrm{eff}} := \lambda + \gamma$ and $\mu_{\mathrm{eff}} := \mu - \gamma$ denote the effective Lamé parameters. The key equation to proceed is the balance of linear momentum (7), linearized at the reference configuration, and subject to the boundary condition (8),

$$\boxed{\mathrm{Div}\boldsymbol{\Sigma} = \boldsymbol{0} \quad \text{in } \mathcal{B}_s \qquad \text{subject to} \qquad \boldsymbol{\Sigma}\cdot\boldsymbol{N} = \boldsymbol{T}^{\mathrm{p}} \quad \text{on } \partial\mathcal{B}_s \qquad \text{with} \quad \boldsymbol{\Sigma} := \gamma\boldsymbol{I} + [\mathbb{C}_{\mathrm{eff}} + \gamma\mathbb{I}] : \nabla\boldsymbol{u}\,.} \tag{16}$$

Remark: Alternative stress measures. *The linearization of the different stress measures provides additional insight in the interpretation of prestress. Although the non-symmetric Piola stress $\boldsymbol{P}$ is the only stress measure relevant to evaluate the balance equation (7), it is possible to compute the corresponding alternative finite deformation stress measures in the context of the infinitesimal deformations. Accordingly, the fully material symmetric Piola–Kirchhoff stress $\boldsymbol{S}$ and the fully spatial symmetric Cauchy stress $\boldsymbol{\sigma}$ can be linearized at $\mathcal{B}_s$,*

$$\mathrm{Lin}\,\boldsymbol{S}|_{\boldsymbol{F}=\boldsymbol{I}} = \boldsymbol{S}|_{\boldsymbol{F}=\boldsymbol{I}} + \frac{\partial \boldsymbol{S}}{\partial \boldsymbol{F}}\Big|_{\boldsymbol{F}=\boldsymbol{I}} : [\boldsymbol{F} - \boldsymbol{I}] = \gamma\boldsymbol{I} + \Big[3[\lambda + \gamma]\mathbb{I}^{\mathrm{vol}} + 2[\mu - \gamma]\mathbb{I}^{\mathrm{sym}}\Big] : \boldsymbol{\epsilon}$$
$$\mathrm{Lin}\,\boldsymbol{\sigma}|_{\boldsymbol{F}=\boldsymbol{I}} = \boldsymbol{\sigma}|_{\boldsymbol{F}=\boldsymbol{I}} + \frac{\partial \boldsymbol{\sigma}}{\partial \boldsymbol{F}}\Big|_{\boldsymbol{F}=\boldsymbol{I}} : [\boldsymbol{F} - \boldsymbol{I}] = \gamma\boldsymbol{I} + \Big[3\lambda\mathbb{I}^{\mathrm{vol}} + 2\mu\mathbb{I}^{\mathrm{sym}}\Big] : \boldsymbol{\epsilon}\,.$$

In the absence of deformation, i.e., for $\nabla\boldsymbol{u} = \boldsymbol{0}$, all stress measures assume the same prestress $\gamma\boldsymbol{I}$. In the absence of the prestress, i.e., for $\gamma = 0$, all linearized stress measures are identical. This is why, with a few exceptions, e.g., Bazant (1971); Hoger (1986), the classical linear elasticity theory typically does not distinguish between the different stress measures. □

4. Stability analysis for prestressed continua

To ensure that the boundary value problem is well-posed, it has to satisfy specific conditions. In the following, we expand the classical condition of strong ellipticity, the classical condition of pointwise stability, and the classical boundary complementing condition originally established for continua without prestress (Marsden and Hughes, 1994) to prestressed continua.

4.1. Strong ellipticity

First, we explore the condition of strong ellipticity in the context of prestress. The elasticity tensor $\mathbb{c}$ is *strongly elliptic*, associated with a real wave speed, if, for all vectors $\boldsymbol{a}, \boldsymbol{b} \neq \boldsymbol{0}$,

$$[\boldsymbol{a} \otimes \boldsymbol{b}] : \mathbb{c} : [\boldsymbol{a} \otimes \boldsymbol{b}] > 0\,. \tag{17}$$

For our particular constitutive model with prestress (9), for which $\mathbb{c} = \mathbb{C}_{\text{eff}} + \gamma\mathbb{I}$, the condition of strong ellipticity translates into the following expression,

$$[\boldsymbol{a} \otimes \boldsymbol{b}] : [\, \mathbb{C}_{\text{eff}} + \gamma\mathbb{I}\,] : [\boldsymbol{a} \otimes \boldsymbol{b}] > 0\,. \tag{18}$$

For the effective tangent moduli $\mathbb{C}_{\text{eff}} = 3\lambda_{\text{eff}}\,\mathbb{I}^{\text{vol}} + 2\mu_{\text{eff}}\,\mathbb{I}^{\text{sym}}$ according to equation (15), this implies that

$$\boxed{\text{strong ellipticity:} \qquad \mu > 0 \quad \text{and} \quad \lambda + 2\mu > 0\,.} \tag{19}$$

Alternatively, we can state the condition of strong ellipticity through the positive-definiteness of the acoustic tensor $\boldsymbol{q}$ defined in terms of the unit vector $\boldsymbol{b}$ with $|\,\boldsymbol{b}\,| = 1$,

$$\det \boldsymbol{q} > 0 \quad \text{with} \quad \boldsymbol{q} := [\boldsymbol{I} \otimes \boldsymbol{b}] : [\, \mathbb{C}_{\text{eff}} + \gamma\mathbb{I}\,] \cdot \boldsymbol{b}. \tag{20}$$

4.2. Pointwise stability

Second, we study the condition of point wise stability in the context of prestress. The elasticity tensor $\mathbb{c}$ is said to be *pointwise stable* if, for all symmetric second order tensors $\boldsymbol{\epsilon} = \boldsymbol{\epsilon}^{\text{t}}$,

$$\boldsymbol{\epsilon} : \mathbb{c} : \boldsymbol{\epsilon} > 0\,. \tag{21}$$

Here, since our constitutive tensor $\mathbb{c} = \mathbb{C}_{\text{eff}} + \gamma\mathbb{I}$ does not possesses minor and major symmetries similar to the classical elasticity tensor $\mathbb{c}$, we cannot simply adapt the classical pointwise stability condition above. Pointwise stability requires the stored energy $\boldsymbol{\sigma} : \delta\boldsymbol{\epsilon}$ to increase for increasing incremental strains $\delta\boldsymbol{\epsilon}$. In our case, pointwise stability translates into the following condition, $\nabla\boldsymbol{u} : [\mathbb{C}_{\text{eff}} + \gamma\mathbb{I}] : \nabla\boldsymbol{u} - \nabla\boldsymbol{u} \cdot \gamma\boldsymbol{I} \cdot \nabla\boldsymbol{u} > 0$, or alternatively, for all displacement gradients $\nabla\boldsymbol{u}$, not necessarily symmetric,

$$\nabla\boldsymbol{u} : \mathbb{C}_{\text{eff}} : \nabla\boldsymbol{u} > 0\,. \tag{22}$$

Here we have assumed that the prestress is subtracted from the total stress $\boldsymbol{\Sigma}$ since it is a priori in balance with externally prescribed tractions $\boldsymbol{T}^{\text{p}}$. Furthermore, we have subtracted the geometrical stiffness term $\nabla\boldsymbol{u} \cdot \gamma\boldsymbol{I} \cdot \nabla\boldsymbol{u}$ to *properly* impose pointwise stability (Hoger, 1995). From $\mathbb{C}_{\text{eff}} = 3\,\lambda_{\text{eff}}\,\mathbb{I}^{\text{vol}} + 2\,\mu_{\text{eff}}\,\mathbb{I}^{\text{sym}}$, we conclude that the pointwise stability condition only affects the symmetric part $\boldsymbol{\epsilon} = \nabla^{\text{sym}}\boldsymbol{u}$ of the displacement gradient $\nabla\boldsymbol{u}$, thus

$$\boldsymbol{\epsilon} : [\, 3\,\lambda_{\text{eff}}\,\mathbb{I}^{\text{vol}} + 2\,\mu_{\text{eff}}\,\mathbb{I}^{\text{sym}}\,] : \boldsymbol{\epsilon} > 0\,. \tag{23}$$

Alternatively, we can reformulate the above equation in terms of volumetric and deviatoric parts,

$$\boldsymbol{\epsilon} : [\, \underbrace{[3\lambda_{\text{eff}} + 2\mu_{\text{eff}}]}_{3\lambda+2\mu+\gamma}\,\mathbb{I}^{\text{vol}} + \underbrace{2\mu_{\text{eff}}}_{2\mu-2\gamma}\,\mathbb{I}^{\text{dev}}\,] : \boldsymbol{\epsilon} > 0\,, \tag{24}$$

where $\mathbb{I}^{\text{dev}} := \mathbb{I}^{\text{sym}} - \mathbb{I}^{\text{vol}}$. With $3\lambda_{\text{eff}} + 2\mu_{\text{eff}} = 3\lambda + 2\mu + \gamma$ and $2\mu_{\text{eff}} = 2\mu - 2\gamma$ this implies that pointwise stability holds within the following prestress limits γ,

$$\boxed{\text{pointwise stability:} \qquad -3\lambda - 2\mu < \gamma < \mu\,.} \tag{25}$$

Since the Lamé parameters $\lambda \geq 0$ and $\mu \geq 0$ are strictly non-negative, the above condition implies that pointwise stability can either be violated by negative growth or shrinkage associated with a tensile prestress $\gamma > \mu$ or by positive growth associated with a compressive prestress $\gamma < -3\lambda - 2\mu$.

4.3. Boundary complementing condition

Third, we study the boundary complementing condition associated with the infinitesimal, quasi-static, incremental boundary value problem. We consider a semi-infinite half-space of bulk material subjected to an incremental deformation $\delta\boldsymbol{u}$ such that the total deformation is $\boldsymbol{u} + \delta\boldsymbol{u}$. The corresponding stress $\boldsymbol{\Sigma} + \delta\boldsymbol{\Sigma}$ has to satisfy the balance equation

and its boundary condition (16), i.e.,

$$\mathrm{Div}\,(\boldsymbol{\Sigma}+\delta\boldsymbol{\Sigma})=\boldsymbol{0}\quad\text{in }\mathcal{B}_s\qquad\text{subject to}\qquad[\boldsymbol{\Sigma}+\delta\boldsymbol{\Sigma}]\cdot\boldsymbol{N}=\boldsymbol{T}^{\mathrm{p}}\quad\text{on }\partial\mathcal{B}_s\,. \tag{26}$$

Since, $\mathrm{Div}\boldsymbol{\Sigma}=\boldsymbol{0}$ and $\boldsymbol{\Sigma}\cdot\boldsymbol{N}=\boldsymbol{T}^{\mathrm{p}}$, the incremental balance of linear momentum in the bulk in the absence of a body force field reduces to the following expression along with its boundary condition,

$$\mathrm{Div}\,\delta\boldsymbol{\Sigma}=\boldsymbol{0}\quad\text{in }\mathcal{B}_s\qquad\text{subject to}\qquad\delta\boldsymbol{\Sigma}\cdot\boldsymbol{N}=\boldsymbol{0}\quad\text{on }\partial\mathcal{B}_s\,. \tag{27}$$

Here, for the case of isotropic volume growth, we assume that the externally prescribed tractions are constant and responsible to map the grown configuration to the stressed configuration, hence $\boldsymbol{T}^{\mathrm{p}}=\gamma\boldsymbol{N}$. The incremental stress tensor $\delta\boldsymbol{\Sigma}$ is related to the incremental deformation tensor $\delta\nabla\boldsymbol{u}$ via the constitutive relation

$$\delta\boldsymbol{\Sigma}:=[\mathbb{C}_{\mathrm{eff}}+\gamma\mathbb{I}]:\delta\nabla\boldsymbol{u}\,. \tag{28}$$

To explore the boundary complementing condition we consider a hypothetical stationary wave on the surface of the bulk half-space as depicted in Figure 4 (Benallal et al., 1993; Utzinger et al., 2008; Javili et al., 2012). The stationary wave lies in the plane spanned by the surface base vectors $\boldsymbol{t}$ and $\boldsymbol{b}$, where $\boldsymbol{b}$ is directed outwards. The wave is constructed to decay towards the bulk such that the decay direction coincides with $\boldsymbol{d}$. In what follows, we denote relevant vectors and tensors by small letters and restrict the displacement increment $\delta\boldsymbol{u}$ to be infinitesimal.
We label the position vector of a point within the bulk with respect to the origin of the local surface orthonormal base system $\boldsymbol{t},\boldsymbol{b},\boldsymbol{d}$ as $\overline{\boldsymbol{x}}$, and denote its projections onto the $\boldsymbol{t}$ and $\boldsymbol{d}$ directions as ξ and η,

$$\xi=\overline{\boldsymbol{x}}\cdot\boldsymbol{d}\qquad\text{and}\qquad\eta=\overline{\boldsymbol{x}}\cdot\boldsymbol{t}\,. \tag{29}$$

We then prescribe a stationary wave-type ansatz for the incremental displacement $\delta\boldsymbol{u}$ as the product of a decay function $\boldsymbol{w}(\xi)$ and a waviness term,

$$\delta\boldsymbol{u}=\boldsymbol{w}(\xi)\,\exp(ik\eta)\,, \tag{30}$$

where $k>0$ is the wave number and i is the imaginary unit. The first and the second gradients of $\delta\boldsymbol{u}$ are denoted as $\nabla\delta\boldsymbol{u}$ and $\nabla_2\delta\boldsymbol{u}$, respectively. We reformulate the incremental balance of linear momentum in the bulk in terms of the incremental displacement $\delta\boldsymbol{u}$ as

$$\mathrm{Div}\delta\boldsymbol{\Sigma}=\mathrm{Div}([\mathbb{C}_{\mathrm{eff}}+\gamma\mathbb{I}]:\delta\nabla\boldsymbol{u})=[[\mathbb{C}_{\mathrm{eff}}+\gamma\mathbb{I}]:\nabla_2\delta\boldsymbol{u}]:\boldsymbol{I}\,. \tag{31}$$

To study the boundary complementing condition on the surface, we consider the incremental balance of linear momentum on the surface (27.2), here simply the incremental boundary condition restated as follows,

$$\widehat{\delta\boldsymbol{\Sigma}}\cdot\boldsymbol{N}=\widehat{\delta\boldsymbol{\Sigma}}\cdot[-\boldsymbol{d}]=\boldsymbol{0}\qquad\text{with}\qquad\widehat{\delta\boldsymbol{\Sigma}}:=\delta\boldsymbol{\Sigma}\Big|_{\xi=0}\,. \tag{32}$$

Here, we have introduced the hat symbol to indicate the evaluation of the corresponding quantity, here the incremental stress $\delta\boldsymbol{\Sigma}$, on the material surface, i.e., at $\xi=0$. Using the incremental constitutive equation (28), together with proper wave-type ansatz governed by incremental balance of momentum in the bulk (31), along with the mathematical transformations detailed in the Appendix, we obtain the following expression

$$\mathbb{B}\cdot\boldsymbol{a}=\boldsymbol{0}\,,\qquad\text{with}\qquad\mathbb{B}:=\begin{bmatrix}-2\mu k+\gamma k & \mu & 0\\ -2\mu k+\gamma k & \lambda+2\mu & 0\\ 0 & 0 & -\mu k\end{bmatrix}\qquad\text{and}\qquad\boldsymbol{a}:=\begin{bmatrix}a_0\\ a_1\\ a_2\end{bmatrix}. \tag{33}$$

Non-trivial solutions of Eq. (33) with $k>0$ correspond to possible stationary surface wave-type solutions of the incremental boundary-value problem. In summary, we can state the condition for a possible bifurcation in the following

form,

$$\boxed{\text{boundary complementing condition:} \qquad \det \mathbb{B} = \mu k^2[\lambda + \mu][2\mu - \gamma] \doteq 0\,.} \tag{34}$$

Remark: Classical case of non-prestressed solids recovered. *For the classical case of a solid without prestress with $\gamma = 0$, Eq. (34) reduces to the classical condition for the loss of the boundary complementing condition,*

$$\det \mathbb{B} = 2\mu^2 k^2[\lambda + \mu] \doteq 0 \quad \Rightarrow \quad \mu = 0 \quad \textit{or} \quad \lambda + \mu = 0\,, \tag{35}$$

which is eliminated a priori because of the pointwise stability of the bulk. □

Remark: Pointwise stability and strong ellipticity eliminate surface bifurcations. *For the case of a solid subjected to prestress with $\gamma > 0$, the conditions for the possible bifurcation with a positive wave number $k > 0$ are*

$$\mu = 0 \qquad \textit{or} \qquad \lambda + \mu = 0 \qquad \textit{or} \qquad 2\mu - \gamma = 0\,, \tag{36}$$

*which are **necessarily** eliminated a priori because of pointwise stability and strong ellipticity. From Eq. (34), we conclude that if a bifurcation does occur, it can have any arbitrary wave number $k > 0$ and any wavelength.* □

5. Examples of growth-induced instabilities

The following examples elucidate the theory presented in the previous sections. First, to investigate the effect of prestress, we illustrate the eigenvalue analysis in the homogeneous setting of a single trilinear finite element. Then, to explore biologically relevant growth, we simulate growth-induced instabilities in the inhomogeneous settings of a hollow cylinder mimicking the airway wall and of a solid half-sphere mimicking the developing brain. Since our main objective is to provide a generic framework for the critical conditions of growth-induced instabilities, we choose arbitrary values for the Lamé parameters of $\mu = 8.0$ and $\lambda = 12.0$ in all four problems.

5.1. Homogeneous problem of eigenvalue analysis for a single trilinear element

To investigate the interplay between negative eigenvalues and bulk prestress γ, we perform a stability analysis for a single trilinear finite element. For simplicity, we assume the dimensions of the element to be unity. The derivation of the underlying weak form and its finite element discretization are standard (Hughes, 1987), except for the local constitutive tensor and the global stiffness matrix, which follow from the boundary value problem (16).

Figure 5 illustrates the eigenvalues of the global stiffness matrix plotted against the prestress. For any prestress level $\gamma > 0$, we obtain six zero eigenvalues, which correspond to three rigid body translations and the three rigid body rotations. According to conditions (19) and (25), at $\gamma = -[3\lambda + 2\mu] = -52$ and at $\gamma = \mu = 8$, the analysis predicts at least one eigenmode associated with a zero eigenvalue, as illustrated in Figure 5. Each of the *predicted* zero energy modes is associated with either a purely volumetric deformation or a purely deviatoric deformation mode. In addition, mixed mode conditions can also result in zero energy modes. In summary, we observe various zero energy modes in addition to the plain modes indicated in conditions (19) and (25).

5.2. Inhomogeneous problem of shrinkage-induced instabilities in a hollow cylinder

The first inhomogeneous example is a shrinking infinitely long hollow cylinder, modeled as a two-dimensional ring under *plane strain* conditions. The ring has an outer diameter of unit length and an inner radius of 0.3. We discretize the geometry using 1920 bilinear quadrilateral finite elements. While we allow the inner boundary to move freely upon growth, we subject the outer boundary to homogeneous Dirichlet boundary conditions. To mimic the effect of *negative growth* or shrinkage, we apply a *tensile prestress* of $\gamma = 9$, a value beyond the critical prestress level of $\gamma = \mu = 8$, as predicted by the pointwise stability condition in equation (25).

Figure 6 illustrates selected instability patterns along with their associated eigenvalues. Tensile prestress beyond the critical limit is associated with shrinkage-induced instabilities. In contrast to many studies in the literature, here, the associated unstable modes of Figure 6 result exclusively from the eigenvalue analysis of the global stiffness matrix

and are not associated with randomly applied perturbations. If we apply a perturbation, we observe mixed instability modes. Our analysis is capable of capturing a tetragonal, pentagonal, hexagonal instability patterns. Without perturbation, it is even possible to see no instabilities at all.

5.3. Inhomogeneous problem of growth-induced instabilities in a hollow cylinder

The second inhomogeneous example is a growing infinitely long hollow cylinder, modeled as a two-dimensional ring under *plane stress* conditions. The ring has an outer diameter of unit length, an inner radius of 0.3, and a thickness of 0.001. We discretize the geometry using 1280 bilinear quadrilateral finite elements. Similar to the previous problem, we allow the inner boundary to move freely upon growth, and subject the outer boundary to homogeneous Dirichlet boundary conditions. To mimic the effect of *positive growth*, we apply a *compressive prestress* of $\gamma = -55$, a value beyond the critical prestress level of $\gamma = -3\lambda - 2\mu = -52$, as predicted by the pointwise stability condition in equation (25).

Figure 7 illustrates selected instability patterns along with their associated eigenvalues. Compressive prestress beyond the critical limit is associated with growth-induced instabilities. Similar to the previous example, our analysis is capable of capturing a hexagonal, heptagonal, and octagonal instability patterns. We observed that, to obtain more unstable modes, we need to either apply a finer discretization or a smaller prestress γ, larger in magnitude and further away from the critical threshold.

5.4. Inhomogeneous problem of growth-induced instabilities in a solid half-sphere

The final example is a growing solid half-sphere in a fully three-dimensional setting. The sphere has a radius of 0.3. We discretize its geometry with 3456 trilinear hexahedral finite elements. We allow the outer boundary to move freely upon growth, fix the center against rigid body translations and rotations, and apply homogeneous Dirichlet boundary conditions in z-direction at the bottom to account for symmetry conditions. To mimic the effect of *positive growth*, we apply a *compressive prestress* of $\gamma = -100$, a value beyond the critical prestress level of $\gamma = -3\lambda - 2\mu = -52$, as predicted by the pointwise stability condition in equation (25).

Figure 8 illustrates selected instability patterns along with their associated eigenvalues. Compressive prestress beyond the critical limit is associated with growth-induced instabilities. Similar to the previous examples, our analysis is capable of capturing different instability patterns associated with the different eigenmodes.

6. Discussion

Many living structures undergo biological growth during development or under diseased conditions. Growth is often the origin for geometric instabilities in the form of folding or wrinkling. Typical examples are folding patterns in the developing brain and wrinkling patterns in chronically obstructed airways. To better understand malformations during development or disease progression, it is important to know when and how these instabilities form. Here we have presented our first attempts to systematically characterize the critical conditions for growth-induced instabilities in living structures.

The classical approach to model biological growth is to kinematically introduce an incompatible growth configuration and to multiplicatively decompose the deformation gradient into an elastic part and a growth part. The key idea of this manuscript is to conceptually replace growth with prestress and establish a generic framework for growth- or rather prestress-induced instabilities. In terms of configurations, we map the stress-free grown configuration onto a stressed configuration, which is *geometrically* identical to the initial configuration before growth. However, this configuration is not stress-free and therefore not *energetically* identical to the initial configuration. This concept allows us to adopt a classical instability analysis, and highlight critical conditions of strong ellipticity and of pointwise stability and the boundary complementing condition.

Our linear stability analysis allows us to predict critical prestress levels for negative growth or shrinkage, associated with a tensile prestress, and for positive growth, associated with compressive prestress. In particular, the pointwise stability condition reveals the critical prestress limits γ under tension and compression as functions of the material parameters λ and μ as $-3\lambda - 2\mu < \gamma < \mu$. The accompanying eigenvalue analysis of the finite-element based global stiffness matrix provides a first insight into the corresponding unstable modes. To study the structural response beyond the onset of instabilities, a natural extension of the proposed work would be to perform a post-buckling analysis based on a fully geometrically non-linear approach.

Under plain strain conditions, our critical condition for growth-induced instabilities is $2\lambda+2\mu = 0$, which is clearly independent of the prestress level γ. At first glance, this condition seems to contradict the literature on growth-induced instabilities in the airway wall (Li et al., 2011). However, there are two major differences between the models in the literature and our model: First, most previously reported geometric models are based on double-layered cylindrical tubes (Cao et al., 2012; Jin et al., 2011), while we have limit our analysis to a single-layered tube (Moulton and Goriely, 2011). Second, and more importantly, most previously reported growth models constrain growth in the axial direction (Moulton and Goriely, 2011a; Li et al., 2011), while we have assumed that a fully three-dimensional growth results in a fully isotropic prestress state. A natural extension of our model would therefore be to incorporate these effects and study whether our approach can generate similar unstable modes under similar conditions.

An exciting extension of the proposed work would be to model surface wrinkling and folding (Zöllner et al., 2012) using the concept of surface tension and surface elasticity (Javili and Steinmann, 2009, 2010a). This could become particularly relevant for thin films as the mucous membrane, whose thickness is orders of magnitude smaller than the structural dimensions of the airway system (Holland et al., 2013; Papastavrou et al., 2013). This line of extension could provide further insight into growth of thin biological membranes, since it would allow the surface to have its own energetic structure (Gurtin and Murdoch, 1975; Javili and Steinmann, 2010b).

To ultimately serve as a predictive diagnostic tool to identify the onset of growth-induces instabilities in living systems, it is critical to experimentally calibrate and validate the underlying growth law. Along these lines, recent studies have characterized growth tensors in the heart wall (Rausch et al., 2011; Tsamis et al., 2012) and in heart valves (Rausch et al., 2012). Using implanted videofluoroscopic markers and biplane imaging, a recent inverse analysis suggested prestrain values of the order of 30-40% in the mitral valve leaflet (Rausch et al., 2013). These studies indicate that it is critically important to include the effects of prestrain or residual stress when studying living systems (Rausch et al., 2013a).

In summary, this manuscript presents our first attempts to shed light on growth-induced instabilities in living structures by conceptually replacing growth through prestress. This allows us to adapt the standard concepts of a classical linear stability analysis and predict the critical prestress levels at which kinematic instabilities may occur. We believe that this generic framework is broadly applicable to enhance our understanding of growth-induced instabilities with clinical applications in plastic and reconstructive surgery, asthma, obstructive sleep apnoea, and brain development.

Acknowledgements

This study was supported in part by the National Science Foundation CAREER award CMMI 0952021 and INSPIRE grant 1233054 and by the National Institutes of Health Grant U54 GM072970.

Appendix

It is enlightening to provide the intermediate steps to study the boundary complementing condition briefly introduced in Sec. 4.3. The position vector of a point within the bulk with respect to the origin of the local surface orthonormal base system $\boldsymbol{t}, \boldsymbol{b}, \boldsymbol{d}$ is denoted $\overline{\boldsymbol{x}}$. The projections of the position vector $\overline{\boldsymbol{x}}$ in the $\boldsymbol{t}$ and $\boldsymbol{d}$ directions are denoted as

$$\xi = \overline{\boldsymbol{x}} \cdot \boldsymbol{d} \qquad \text{and} \qquad \eta = \overline{\boldsymbol{x}} \cdot \boldsymbol{t} \,. \tag{37}$$

A stationary wave-type ansatz for the incremental displacement $\delta\boldsymbol{u}$ is prescribed as the product of a decay function $\boldsymbol{w}(\xi)$ and a waviness term,

$$\delta\boldsymbol{u} = \boldsymbol{w}(\xi) \exp(ik\eta) \,, \tag{38}$$

where $k > 0$ is the wave number and i is the imaginary unit. The first and the second gradients of $\delta\boldsymbol{u}$ are thus given by

$$\nabla\delta\boldsymbol{u} = [\boldsymbol{w}' \otimes \boldsymbol{d} + ik\boldsymbol{w} \otimes \boldsymbol{t}] \exp(ik\eta) \,,$$
$$\nabla_2\delta\boldsymbol{u} = [\boldsymbol{w}'' \otimes \boldsymbol{d} \otimes \boldsymbol{d} + ik[\boldsymbol{w}' \otimes \boldsymbol{t} \otimes \boldsymbol{d} + \boldsymbol{w}' \otimes \boldsymbol{d} \otimes \boldsymbol{t}]] \exp(ik\eta) - [k^2\boldsymbol{w} \otimes \boldsymbol{t} \otimes \boldsymbol{t}] \exp(ik\eta).$$

The incremental balance of momentum in the bulk can be related to the incremental displacement $\delta\boldsymbol{u}$ as

$$\mathrm{Div}\delta\boldsymbol{\Sigma} = \mathrm{Div}([\mathbb{C}_{\mathrm{eff}} + \gamma\mathbb{I}] : \delta\nabla\boldsymbol{u}) = [[\mathbb{C}_{\mathrm{eff}} + \gamma\mathbb{I}] : \nabla_2\delta\boldsymbol{u}] : \boldsymbol{I}\,. \tag{39}$$

Equation (39) yields the ordinary differential equation

$$\boldsymbol{q}_2 \cdot \boldsymbol{w}'' + ik\boldsymbol{q}_1 \cdot \boldsymbol{w}' - k^2\boldsymbol{q}_0 \cdot \boldsymbol{w} = \boldsymbol{0}\,, \tag{40}$$

for the decay function $\boldsymbol{w}(\xi)$ where the localization tensors $\boldsymbol{q}_0$, $\boldsymbol{q}_1$ and $\boldsymbol{q}_2$ are defined by

$$\begin{aligned}
\boldsymbol{q}_0 \cdot \{\bullet\} &:= [[\mathbb{C}_{\mathrm{eff}} + \gamma\mathbb{I}] : [\{\bullet\} \otimes \boldsymbol{t}]] \cdot \boldsymbol{t}\,,\\
\boldsymbol{q}_1 \cdot \{\bullet\} &:= [[\mathbb{C}_{\mathrm{eff}} + \gamma\mathbb{I}] : [\{\bullet\} \otimes \boldsymbol{d}]] \cdot \boldsymbol{t} + [[\mathbb{C}_{\mathrm{eff}} + \gamma\mathbb{I}] : [\{\bullet\} \otimes \boldsymbol{t}]] \cdot \boldsymbol{d}\,,\\
\boldsymbol{q}_2 \cdot \{\bullet\} &:= [[\mathbb{C}_{\mathrm{eff}} + \gamma\mathbb{I}] : [\{\bullet\} \otimes \boldsymbol{d}]] \cdot \boldsymbol{d}\,.
\end{aligned}$$

The decay function $\boldsymbol{w}(\xi)$ can be expressed as

$$\boldsymbol{w}(\xi) = \boldsymbol{m}\exp(\tau\xi)\,, \tag{41}$$

where $\boldsymbol{m}$ is the amplitude of the wave and $\tau < 0$ is the decay exponent. Thus Eq. (40) can be written as

$$[\tau^2\boldsymbol{q}_2 + i\tau k\boldsymbol{q}_1 - k^2\boldsymbol{q}_0] \cdot \boldsymbol{m} =: \boldsymbol{q}_s \cdot \boldsymbol{m} = \boldsymbol{0}\,,$$

or alternatively in a form without the localization tensors as

$$[[\mathbb{C}_{\mathrm{eff}} + \gamma\mathbb{I}] : [\boldsymbol{m} \otimes [k\boldsymbol{t} - i\tau\boldsymbol{d}]]] \cdot [k\boldsymbol{t} - i\tau\boldsymbol{d}] =: \boldsymbol{q}_s \cdot \boldsymbol{m} = \boldsymbol{0}\,,$$

where $\boldsymbol{q}_s$ denotes the surface localization tensor. The decay exponent τ corresponding to non-trivial solutions for the amplitude $\boldsymbol{m}$ are given by

$$\tau = \arg(\det \boldsymbol{q}_s \equiv 0)\,. \tag{42}$$

Equation (42) states the necessary conditions for the possibility of stationary wave-type solutions on the surface. Thus, Eq. (41) can be expressed in the following general form for distinct τ_i and $\boldsymbol{m}_i$ with the coefficients a_i dependent on the boundary conditions,

$$\boldsymbol{w}(\xi) = \sum_{i=0}^{2} a_i\boldsymbol{m}_i \exp(\tau_i\xi)\,. \tag{43}$$

The performed analysis so far, does not require the bulk to be isotropic, nevertheless, in the remainder of this work we apply the analysis to the special case of isotropy. For the case of isotropic, linear elasticity the bulk localization tensors $\boldsymbol{q}_0$, $\boldsymbol{q}_1$ and $\boldsymbol{q}_2$ simplify to

$$\begin{aligned}
\boldsymbol{q}_0 &= [\lambda_{\mathrm{eff}} + \mu_{\mathrm{eff}}]\boldsymbol{t} \otimes \boldsymbol{t} + \mu_{\mathrm{eff}}\boldsymbol{i} + \gamma\boldsymbol{i} = [\lambda + \mu]\boldsymbol{t} \otimes \boldsymbol{t} + \mu\boldsymbol{i}\,,\\
\boldsymbol{q}_1 &= [\lambda + \mu][\boldsymbol{d} \otimes \boldsymbol{t} + \boldsymbol{t} \otimes \boldsymbol{d}]\,,\\
\boldsymbol{q}_2 &= [\lambda_{\mathrm{eff}} + \mu_{\mathrm{eff}}]\boldsymbol{d} \otimes \boldsymbol{d} + \mu_{\mathrm{eff}}\boldsymbol{i} + \gamma\boldsymbol{i} = [\lambda + \mu]\boldsymbol{d} \otimes \boldsymbol{d} + \mu\boldsymbol{i}\,.
\end{aligned}$$

In particular the bulk acoustic (localization) tensor, defined by $\boldsymbol{q}_b := \boldsymbol{q}_2$, can be reformulated as

$$\boldsymbol{q}_b = [\lambda + 2\mu]\boldsymbol{d} \otimes \boldsymbol{d} + \mu\boldsymbol{t} \otimes \boldsymbol{t} + \mu\boldsymbol{b} \otimes \boldsymbol{b}\,.$$

Note that any contribution from the prestress γ eventually vanishes in the definitions of the acoustic tensor and this is expected since the acoustic tensors are representing the material behaviour and not its loading conditions. It is clear from the strong ellipticity of the bulk, detailed in Sec. 4.1, that the coefficients $[\lambda + 2\mu]$ and μ will be strictly positive.

The determinant of the surface localization tensor, which vanishes for non-trivial solutions, is given by

$$\det \boldsymbol{q}_s = [k^2 - \tau^2]^3 \underbrace{\mu^2[\lambda + 2\mu]}_{\det \boldsymbol{q}_b \neq 0} \doteq 0 \tag{44}$$

which corresponds to the triple roots $\tau = \pm k$. In order to have bounded solutions, only negative values of the decay exponent τ are admissible, and hence $\tau \equiv -k$. Thus by manipulating Eq. (43) the decay function reads

$$\boldsymbol{w}(\xi) = [[\boldsymbol{t} + i\boldsymbol{d}][a_0 + a_1\xi] + \boldsymbol{b}a_2] \exp(-k\xi) \,. \tag{45}$$

The decay function is then inserted into stationary wave-type ansatz (38) which yields the following expression for the incremental displacement and its gradient,

$$\begin{aligned}
\delta\boldsymbol{u} &= \boldsymbol{w}(\xi) \exp(ik\eta) = [[\boldsymbol{t} + i\boldsymbol{d}][a_0 + a_1\xi] + \boldsymbol{b}a_2] \exp(k[i\eta - \xi]) \,, \\
\nabla\delta\boldsymbol{u} &= [[\boldsymbol{t} + i\boldsymbol{d}][a_1 - k[a_0 + a_1\xi]] - \boldsymbol{b}ka_2] \exp(k[i\eta - \xi]) \otimes \boldsymbol{d} + \; ik[[\boldsymbol{t} + i\boldsymbol{d}][a_0 + a_1\xi] + \boldsymbol{b}a_2] \exp(k[i\eta - \xi]) \otimes \boldsymbol{t} \,.
\end{aligned}$$

In order to study the boundary complementing condition on the surface, consider the incremental balance of linear momentum at the surface (27), here simply the incremental boundary condition, restated as

$$\widehat{\delta\boldsymbol{\Sigma}} \cdot \boldsymbol{N} = \widehat{\delta\boldsymbol{\Sigma}} \cdot [-\boldsymbol{d}] = \boldsymbol{0} \qquad \text{with} \qquad \widehat{\delta\boldsymbol{\Sigma}} := \delta\boldsymbol{\Sigma}\Big|_{\xi=0} \,, \tag{46}$$

where the evaluation of the incremental stress in the bulk at the surface, i.e., $\xi = 0$, is denoted by a hat above the stress. Employing the aforementioned constitutive assumptions and incremental constitutive law (28) in the bulk yields

$$\widehat{\delta\boldsymbol{\Sigma}} = [\mathbb{C}_{\text{eff}} + \gamma\mathbb{I}] : \widehat{\delta\nabla\boldsymbol{u}} \qquad \text{with} \qquad \widehat{\delta\nabla\boldsymbol{u}} := \delta\nabla\boldsymbol{u}\Big|_{\xi=0} \,. \tag{47}$$

The evaluation of the incremental displacement and its first gradient at the surface are given by

$$\begin{aligned}
\widehat{\delta\boldsymbol{u}} &:= \delta\boldsymbol{u}|_{\xi=0} = \boldsymbol{w}(0) \exp(ik\eta) = [a_0[\boldsymbol{t} + i\boldsymbol{d}] + a_2\boldsymbol{b}] \exp(ik\eta) \,, \\
\widehat{\nabla\delta\boldsymbol{u}} &= \nabla\delta\boldsymbol{u}|_{\xi=0} = [[\boldsymbol{t} + i\boldsymbol{d}][a_1 - ka_0] - \boldsymbol{b}ka_2] \otimes \boldsymbol{d} \exp(ik\eta) + \; ik[[\boldsymbol{t} + i\boldsymbol{d}]a_0 + \boldsymbol{b}a_2] \otimes \boldsymbol{t} \exp(ik\eta) \,.
\end{aligned} \tag{48}$$

Note that the evaluation of the displacement gradient at the surface is not, in general, equal to the gradient of the displacement evaluated at the surface, i.e.,

$$\widehat{\nabla\delta\boldsymbol{u}} = \nabla\delta\boldsymbol{u}|_{\xi=0} \neq \nabla\widehat{\delta\boldsymbol{u}} = \nabla\left(\delta\boldsymbol{u}|_{\xi=0}\right) \,.$$

With these definitions at hand, and using Eq. (47), the left-hand side of the incremental balance of linear momentum at the surface (46) is computed next and is eventually set to zero. Inserting Eq. (47) into Eq. (48), yields the following expression for the incremental stress at the surface,

$$\begin{aligned}
\widehat{\delta\boldsymbol{\Sigma}} &= [\mathbb{C}_{\text{eff}} + \gamma\mathbb{I}] : \widehat{\delta\nabla\boldsymbol{u}} \\
&= \left[3\lambda_{\text{eff}}\,\mathbb{I}^{\text{vol}} + 2\mu_{\text{eff}}\,\mathbb{I}^{\text{sym}} + \gamma\mathbb{I}\right] : \left[\,[[\boldsymbol{t} + i\boldsymbol{d}][a_1 - ka_0] - \boldsymbol{b}ka_2] \otimes \boldsymbol{d} + \; ik\,[[\boldsymbol{t} + i\boldsymbol{d}]a_0 + \boldsymbol{b}a_2] \otimes \boldsymbol{t}\right] \exp(ik\eta) \,.
\end{aligned}$$

Next, the quantity $\widehat{\delta\boldsymbol{\Sigma}} \cdot \boldsymbol{d}$ is computed and set to zero.

$$\widehat{\delta\boldsymbol{\Sigma}} \cdot \boldsymbol{d} = \left[\lambda_{\text{eff}} i a_1 \boldsymbol{d} + \mu_{\text{eff}}[[a_1 - ka_0]\boldsymbol{t} + 2i[a_1 - ka_0]\boldsymbol{d} - ka_2\boldsymbol{b} - ka_0\boldsymbol{t}] + \gamma[[\boldsymbol{t} + i\boldsymbol{d}][a_1 - ka_0] - ka_2\boldsymbol{b}]\right] \exp(ik\eta) = \boldsymbol{0} \,,$$

which after some mathematical steps can be reformulated as

$$[\mu[a_1 - 2ka_0] + \gamma ka_0]\boldsymbol{t} + i[\lambda a_1 + 2\mu[a_1 - ka_0] + \gamma ka_0]\boldsymbol{d} + [\,-\mu ka_2]\boldsymbol{b} = \boldsymbol{0} \,,$$

or alternatively in matrix format as

$$\mathbb{B} \cdot \boldsymbol{a} = \mathbf{0} \qquad \text{where} \qquad \mathbb{B} := \begin{bmatrix} -2\mu k + \gamma k & \mu & 0 \\ -2\mu k + \gamma k & \lambda + 2\mu & 0 \\ 0 & 0 & -\mu k \end{bmatrix} \qquad \text{and} \qquad \boldsymbol{a} := \begin{bmatrix} a_0 \\ a_1 \\ a_2 \end{bmatrix}. \tag{49}$$

References

Ambrosi, D., Ateshian, G.A., Arruda, E.M., Cowin, S.C., Dumais, J., Goriely, A., Holzapfel, G.A., Humphrey, J.D., Kemkemer, R., Kuhl, E., Olberding, J.E., Taber, L.A., Garikipati, K., 2011. Perspectives on biological growth and remodeling. Journal of the Mechanics and Physics of Solids 59, 863–883.

Balbi, V., Ciarletta, P., 2013. Morpho-elasticity of intestinal villi. Interface, doi:10.1098/rsif.2013.0109.

Bayly, P.V., Taber, L.A., Kroenke, C.D., 2013. Mechanical forces in cerebral cortical folding: a review of measurements and models. Journal of the Mechanical Behavior of Biomedical Materials, this issue.

Bazant, Z. P., 1971. A correlation study of formulations of incremental deformation and stability of continuous bodies. Journal of Applied Mechanics 38, 919–928.

Benallal, A., Berstad, T., Borvik, T., Hopperstad, O. S., 2010. Uniqueness, loss of ellipticity and localization for the time-discretized, rate-dependent boundary value problem with softening. International Journal For Numerical Methods In Engineering 84 (7), 864–882.

Benallal, A., Billardon, R., Geymonat, G., 1993. Bifurcation and localization in rate-independent materials. Some General Considerations. In: Bifurcation and Stability of Dissipative Systems CISM Courses and Lectures, vol. 327. Springer, pp. 1–44.

Ben Amar, M., Goriely, A., 2005. Growth and instability in elastic tissues. Journal of the Mechanics and Physics of Solids. 53: 2284–2319.

Bharatha, S., Levinson, M., 1978. Signorini's perturbation scheme for a general reference configuration in finite elastostatics. Archive for Rational Mechanics and Analysis 67 (4), 365–394.

Biot, M., 1939. Xliii. non-linear theory of elasticity and the linearized case for a body under initial stress. Philosophical Magazine Series 7 27 (183), 468–489.

Buganza Tepole, A., Ploch, C.J., Wong, J., Gosain, A.K., Kuhl, E., 2011. Growing skin - A computational model for skin expansion in reconstructive surgery. Journal of the Mechanics and Physics of Solids. 59, 2177–2190.

Cao, Y.P., Li, B., Feng, X.Q., 2012. Surface wrinkling and folding of core-shell soft cylinders. Soft Matter. 8, 556–562.

Capriz, G., Guidugli, P. P., 1979. The role of fredholm conditions in signorin's perturbation method. Archive for Rational Mechanics and Analysis 70 (3), 261–288.

Ciarletta, P., Ben Amar, M., 2012. Growth instabilities and folding in tubular organs. A variational method in non-linear elasticity. International Journal of Non-Linear Mechanics. 47, 248–257.

Dowaikh, M. A., Ogden, R. W., 1990. On surface waves and deformations in a pre-stressed incompressible elastic solid. IMA Journal of Applied Mathematics 44 (3), 261–284.

Fung, Y.C. What are the residual stresses doing in our blood vessels *Annals of Biomedical Engineering* 19:237-249,1991.

Garikipati, K., 2009. The kinematics of biological growth. Applied Mechanics Reviews 62, 030801.1–030801.7.

Göktepe, S., Abilez, O.J., Parker, K.K., Kuhl, E., 2010. A multiscale model for eccentric and concentric cardiac growth through sarcomerogenesis. Journal of Theoretical Biology 265, 433–442.

Göktepe, S., Abilez, O.J., Kuhl, E., 2010. A generic approach towards finite growth with examples of athlete's heart, cardiac dilation, and cardiac wall thickening. Journal of the Mechanics and Physics of Solids 58, 1661–1680.

Goriely, A., BenAmar, M., 2005. Differential growth and instability in elastic shells. Physical Review Letters 94 198103.

Gurtin, M. E., Murdoch, A. I., 1975. A continuum theory of elastic material surfaces. Archive for Rational Mechanics and Analysis 57 (4), 291–323.

Hill, R., 1957. On uniqueness and stability in the theory of finite elastic strain. Journal of the Mechanics and Physics of Solids 5 (4), 229–241.

Hill, R., 1958. A general theory of uniqueness and stability in elastic-plastic solids. Journal of the Mechanics and Physics of Solids 6 (3), 236–249.

Himpel, G., Kuhl, E., Menzel, A., Steinmann, P., 2005. Computational modeling of isotropic multiplicative growth. Computational Modeling in Engineering Sciences 8, 119–134.

Hoger, A., 1986. On the determination of residual stress in an elastic body. Journal of Elasticity 16 (3), 303–324.

Hoger, A., 1993. Residual stress in an elastic body: a theory for small strains and arbitrary rotations. Journal of Elasticity 31 (1), 1–24.

Hoger, A., 1995. Positive definiteness of the elasticity tensor of a residually stressed material. Journal of Elasticity 36 (3), 201–226.

Holland MA, Kosmata T, Goriely A, Kuhl E., 2013. On the mechanics of thin films and growing surfaces. Mathematics and Mechanics of Solids. in press.

Hughes, T. J. R., 1987. The finite element method: linear static and dynamic finite element analysis. Vol. 65. Prentice Hall, Inc., Englewood Cliffs N.J.

Javili, A., McBride, A., Steinmann, P., Reddy, B. D., 2012. Relationships between the admissible range of surface material parameters and stability of linearly elastic bodies. Philosophical Magazine.

Javili, A., Steinmann, P., 2009. A finite element framework for continua with boundary energies. Part I: The two-dimensional case. Computer Methods in Applied Mechanics and Engineering 198 (27-29), 2198–2208.

Javili, A., Steinmann, P., 2010a. A finite element framework for continua with boundary energies. Part II: The three-dimensional case. Computer Methods in Applied Mechanics and Engineering 199 (9-12), 755–765.

Javili, A., Steinmann, P., 2010b. On thermomechanical solids with boundary structures. International Journal of Solids and Structures 47 (24), 3245–3253.

Jin, L., Cai, S., Suo, Z., 2011. Creases in soft tissues generated by growth. EPL Frontiers of Physics 95, 64002.1–64002.6.

Johnson, B. E., Hoger, A., 1993. The dependence of the elasticity tensor on residual stress. Journal of Elasticity 33, 145–165.

Li, B., Cao, Y.-P., Feng, X.-Q., Gao, H., 2011. Surface wrinkling of mucosa induced by volumetric growth: Theory, simulation and experiment. Journal of the Mechanics and Physics of Solids 59 (4), 758–774.
Li, B., Cao, Y.P., Feng, X.Q., Gao, H. 2012. Mechanics of morphological instabilities and surface wrinkling in soft materials: A review. Soft Matter 8, 5728–5745.
Man, C. S., Carlson, D. E., 1994. On the traction problem of dead loading in linear elasticity with initial stress. Archive for Rational Mechanics and Analysis 128, 223–247.
Marlow, R. S., 1992. On the stress in an internally constrained elastic material. Journal of Elasticity, 97–131.
Marsden, J. E., Hughes, T. J. R., 1994. Mathematical Foundations of Elasticity. Dover Publications.
Menzel, A., 2005. Modelling of anisotropic growth in biological tissues - A new approach and computational aspects. Biomechanics and Modeling in Mechanobiology 3, 147–171.
Menzel, A., Kuhl, E., 2012. Frontiers in growth and remodeling. Mechanics Research Communications 42, 1–14.
Moulton, D.E., Goriely, A., 2011. Circumferential buckling instability of a growing cylindrical tube. Journal of the Mechanics and Physics of Solids 59, 525–537.
Moulton, D.E., Goriely, A., 2011. Possible role of differential growth in airway wall remodeling in asthma. Journal of Applied Physiololgy 110, 1003–1012.
Ogden, R., 1992. Nonlinear elasticity: Incremental equations and bifurcation phenomena. In: Ames, W., Rogers, C. (Eds.), Nonlinear Equations in the Applied Sciences. Vol. 185 of Mathematics in Science and Engineering. Elsevier, pp. 437–468.
Ogden, R., 2003. Nonlinear elasticity, anisotropy, material stability and residual stresses in soft tissue. In: Holzapfel, G., Ogden, R. (Eds.), Biomechanics of Soft Tissue in Cardiovascular Systems. No. 441 in CISM Courses and Lectures. Springer-Verlag, pp. 65–108.
Papastavrou, A., Steinmann, P., Kuhl, E., 2013. On the mechanics of continua with boundary energies and growing surfaces. Journal of the Mechanics and Physics of Solids. in press. doi:10.1016/j.jmps.2013.01.007.
Rausch, M.K., Dam, A., Göktepe, S., Abilez, O.J., Kuhl, E., 2011. Computational modeling of growth: Systemic and pulmonary hypertension in the heart. Biomechanics and Modeling in Mechanobiology 10, 799–811.
Rausch, M.K., Tibayan, F.A., Miller, D.C., Kuhl, E., 2012. Evidence of adaptive mitral leaflet growth. Journal of the Mechanical Behavior of Biomedical Materials 15, 208–217.
Rausch, M.K., Famaey, N., O'Brien Shultz, T., Bothe, W., Miller, D.C., Kuhl, E., 2013. Mechanics of the mitral valve: A critical review, an in vivo parameter identification, and the effect of prestrain. Biomechanics and Modeling in Mechanobiology, doi:10.1007/s10237-012-0462-z.
Rausch, M.K., Kuhl, E., 2013. On the effect of prestrain and residual stress in thin biological membranes. submitted for publication.
Reddy, B. D., 1982. Surface instabilities on an equibiaxially stretched elastic half-space. Mathematical Proceedings of the Cambridge Philosophical Society 91, 491–501.
Reddy, B. D., 1983. The occurrence of surface instabilities and shear bands in plane strain deformation of an elastic half-space. Quarterly Journal of Mechanics and Applied Mathematics 36, 337–350.
Rodriguez, E. K., Hoger, A., McCulloch, A. D., 1994. Stress-dependent finite growth in soft elastic tissues. Journal of Biomechanics 27 (4), 455–467.
Simpson, H. C., Spector, S. J., 1985. On failure of the complementing condition and nonuniqueness in linear elastostatics. Journal of Elasticity 15, 229–231.
Steinmann, P., 2008. On boundary potential energies in deformational and configurational mechanics. Journal of the Mechanics and Physics of Solids 56, 772–800.
Taber, L.A., 1995. Biomechanics of growth, remodeling and morphogenesis. Applied Mechanics Reviews, 48, 487–545.
Tsamis, A., Cheng, A., Nguyen, T.C., Langer, F., Miller, D.C., Kuhl, E., 2012. Kinematics of cardiac growth - In vivo characterization of growth tensors and strains. Journal of the Mechanical Behavior of Biomedical Materials 8, 165–177.
Utzinger, J., Menzel, A., Steinmann, P., Benallal, A., 2008. Aspects of bifurcation in an isotropic elastic continuum with orthotropic inelastic interface. European Journal of Mechanics - A/Solids 27 (4), 532–547.
Vandiver, R., Goriely, A., 2009. Differential growth and residual stress in cylindrical elastic structures. Philosophical Transactions of the Royal Society A 367, 3607–3630.
Wan, Y. H., Marsden, J. E., 1983. Symmetry and bifurcation in three-dimensional elasticity. Part iii: Stressed reference configurations. Archive for Rational Mechanics and Analysis 84 (3), 203–233.
Wiggs, B.R., Hrousis, C.A., Drazen, J.M., Kamm, R.D., 1997. On the mechanism of mucosal folding in normal and asthmatic airways. Journal of Applied Physiology 83, 1814–1821.
Xie, W.-H., Li, B., Cao, Y.-P., Feng, X.-Q., 2013. Effects of internal pressure and surface tension on the growth-induced wrinkling of mucosae. Journal of the Mechanical Behavior of Biomedical Materials, this issue.
Zöllner, A.M., Buganza Tepole, A., Kuhl, E. 2012 On the biomechanics and mechanobiology of growing skin. Journal of Theoretical Biology 297, 166–175.
Zöllner, A.M., Abilez, O.J., Böl, M., Kuhl, E., 2012. Stretching skeletal muscle: Chronic muscle lengthening through sarcomerogenesis. PLoS ONE 7(10), e45661.

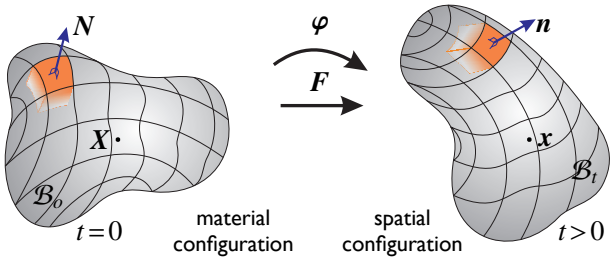

Figure 1: The material and spatial configurations of a continuum body, and the associated motions and deformation gradients.

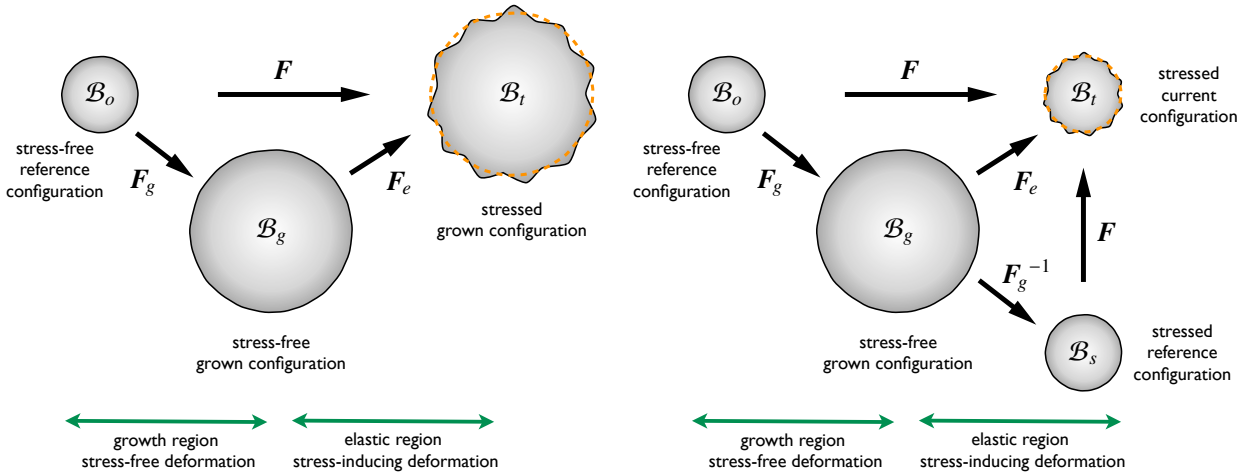

Figure 2: Illustration of kinematics of growth. The classical approach (left) is based on the multiplicative decomposition of the deformation gradient $\boldsymbol{F}$ into an elastic part $\boldsymbol{F}_e$ and a growth part $\boldsymbol{F}_g$. Instability analysis based on this approach is rather complex and it accounts for geometrically induced instabilities which are not the purpose of this manuscript. The current approach (right) modifies the classical decomposition through the inverse mapping $\boldsymbol{F}_g{}^{-1}$. Instability analysis based on the current approach is straightforward and focuses on materially induced instabilities. The admissible range for material parameters and growth can be precisely predicted for the general case.

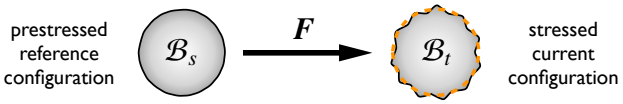

Figure 3: Deformation of the prestressed configuration via the total deformation gradient $\boldsymbol{F} = \boldsymbol{I} + \nabla \boldsymbol{u}$.

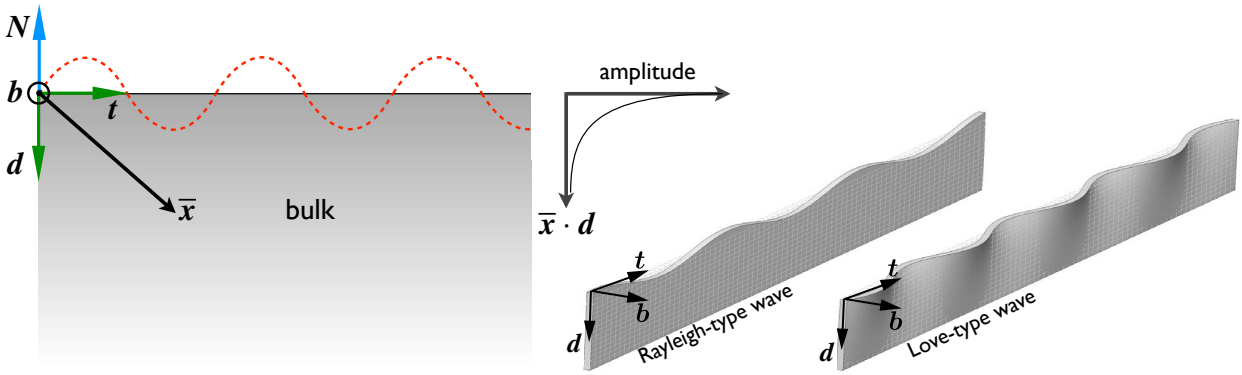

Figure 4: Illustration of the surface wave-type ansatz.

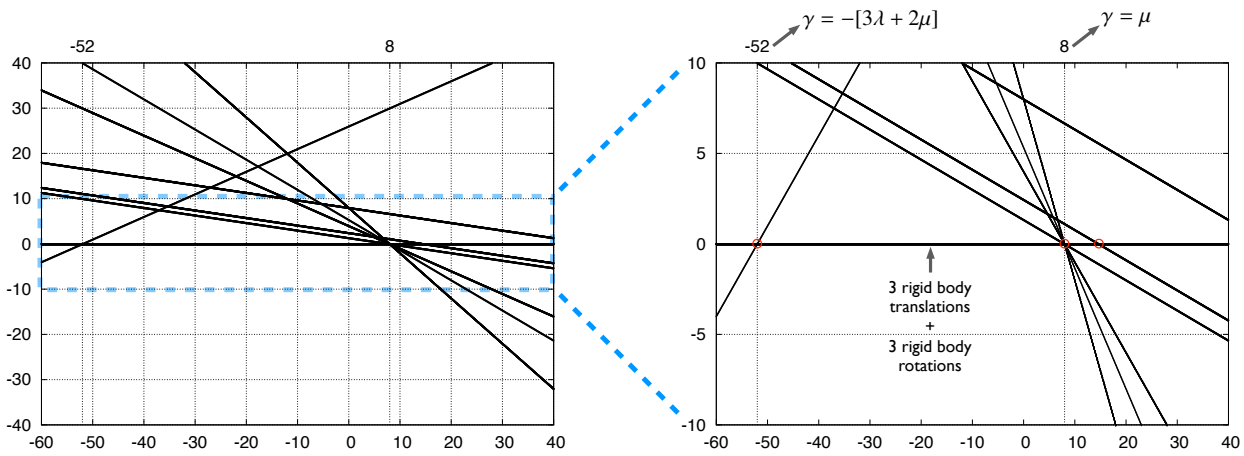

Figure 5: Homogeneous problem of eigenvalue analysis for a single trilinear element. Eigenvalues are plotted versus varying prestress levels γ. Negative eigenvalues are associated with unstable eigenmodes. Circles indicate when an eigenmode reaches its critical condition and becomes unstable.

Figure 6: Inhomogeneous problem of shrinkage-induced instabilities in a hollow cylinder. Selected unstable eigenmodes resulte from a tensile prestress of $\gamma = 9$ beyond the critical stable prestress threshold of $\mu = 8$. Numbers indicate the associated eigenvalues.

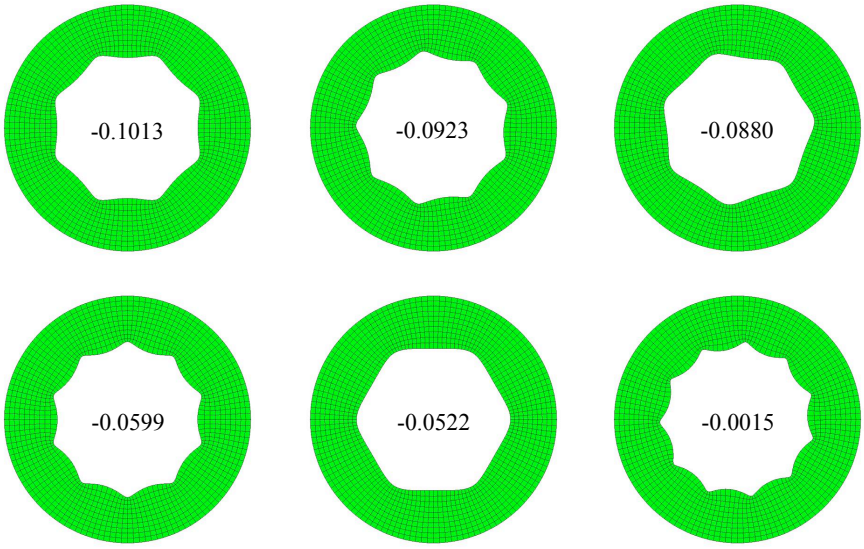

Figure 7: Inhomogeneous problem of growth-induced instabilities in a hollow cylinder. Selected unstable eigenmodes resulte from a compressive prestress of $\gamma = -55$ beyond the critical stable prestress threshold of $-3\lambda - 2\mu = -52$. Numbers indicate the associated eigenvalues multiplied by the inverse of the thickness.

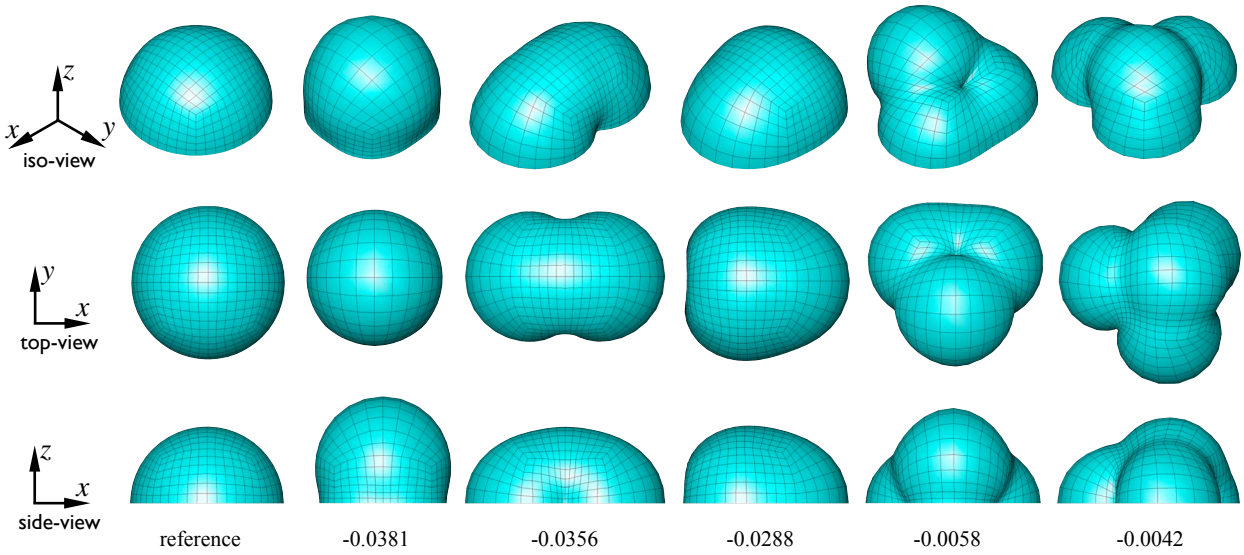

Figure 8: Inhomogeneous problem of growth-induced instabilities in a solid half-sphere. Selected unstable eigenmodes resulte from a compressive prestress of $\gamma = -100$ beyond the critical stable prestress threshold of $-3\lambda - 2\mu = -52$. Numbers indicate the associated eigenvalues.